Unexpected spatial distribution of bubble rearrangements in coarsening foams†‡

David A. Sessoms,[a] Hugo Bissig,[a] Agnès Duri,[b] Luca Cipelletti[b] and Véronique Trappe*[a]

Foams are ideal model systems to study stress-driven dynamics, as stress-imbalances within the system are continuously generated by the coarsening process, which, unlike thermal fluctuations, can be conveniently quantified by optical means. However, the high turbidity of foams generally hinders the detailed study of the temporal and spatial distribution of topological bubble rearrangement events, such that definite assessments regarding their contribution to the overall dynamics could not be made so far. In this paper, we use novel light scattering techniques to measure the frequency and position of events within a large sample volume. As recently reported (A. S. Gittings and D. J. Durian, *Phys. Rev. E*, 2008, **78**, 066313), we find that the foam dynamics is determined by two distinct processes: intermittent bubble rearrangements of finite duration and a spatially homogeneous quasi-continuous process. Our experiments show that the convolution of these two processes precludes assessing the relation between intermittent rearrangements and coarsening process considering solely the mean dynamics. By contrast, the use of the recently introduced photon correlation imaging technique (A. Duri, D. A. Sessoms, V. Trappe, and L. Cipelletti, *Phys. Rev. Lett.*, 2009, **102**, 085702) enables us to ascertain that the event frequency is directly determined by the strain-rate imposed by the coarsening process. Surprisingly, we also find that, although the distribution of successive events in time is consistent with a random process, the spatial distribution of successive events is not random: rearrangements are more likely to occur within a recently rearranged zone. This implies that an unstable local stress configuration that is reconfigured remains intrinsically unstable after the rearrangement has occurred.

1 Introduction

Foams consist of gas bubbles that are densely packed in a continuous liquid phase. Because of the high packing fraction, the bubbles are deformed, such that the system is constantly under internal stress. Though thermal motion is insufficient to lead to any significant restructuring of the random bubble configuration, foams reconfigure in time because of coarsening: larger bubbles growing at the expense of the smaller ones due to the difference in their Laplace pressures. This process leads to imbalances of the internal stresses, which are released by intermittent, local rearrangements of bubbles.[1,2] Thus, the coarsening process provides the system with an internal mechanical means of "thermalization" that eventually allows for a complete reconfiguration of the foam. Such stress-driven relaxation is the hallmark of a variety of other soft glassy systems,[3] such as colloidal gels,[4] concentrated microgel systems,[5] and surfactant phases;[6] however, in these systems, the mechanism leading to unbalanced stresses is not well understood. By contrast, in foams the coarsening process is a quantifiable measure of the temporal evolution of stress-imbalances, and thus foams are ideal benchmark systems to study stress driven relaxation processes.

Their dynamics has been previously investigated using diffusing-wave spectroscopy (DWS),[2,7–12] an extension of dynamic light scattering to the multiple scattering limit.[13,14] However, traditional DWS relies on extensive time and space averaging, thereby precluding direct characterization of the intermittent dynamics. Indeed, recent speckle visibility experiments revealed that the dynamics of foams exhibit features that were not considered in previous modelling of the time-averaged correlation functions.[15] In particular, it was shown that the dynamic light scattering signal was not only determined by intermittent rearrangements of the local bubble configuration, but that another process of undefined origin was contributing as well. Such mix of dynamic processes, however, significantly complicates the interpretation of time and space averaged dynamic light scattering signals that have been used so far to characterize foam dynamics. In particular, it obscures the evaluation of the relation between the intermittent restructuring events and the coarsening process, which is essential to understand the interplay between stress accumulation, local yielding and structural relaxation.

[a]*University of Fribourg, Dept. of Physics, Chemin du Musée 3, CH-1700 Fribourg, Switzerland. E-mail: Veronique.Trappe@unifr.ch*
[b]*LCVN UMR 5587, CNRS and University of Montpellier II, 26 Place E. Bataillon, F-34095 Montpellier, France*

† Electronic supplementary information (ESI) available: Movies showing the evolution of the spatially resolved dynamical activity of Gillette shaving foam at age 1 (movie 1) and age 2 (movie 2). The scale bars correspond to 1 mm. The observational volumes are respectively $V_{sc} = 67$ mm^3 and $V_{sc} = 144$ mm^3 for the experiments at age 1 and age 2. The number of the dynamical independent zones within the observational volume, $V_{sc}/(^4/_3\ \pi\ \xi^3)$, is by a factor of 1.6 higher in the experiment at age 1 than in the experiment at age 2. See DOI: 10.1039/b926873a

In this contribution, we extend the investigations of foam dynamics to spatially resolved dynamics, applying the recently introduced photon correlation imaging scheme[16] to the back-scattering plane of a coarsening foam. To correlate our findings to previous work, we simultaneously perform time resolved experiments[17,18] in the classical transmission far field geometry of DWS. Our results reveal that the event frequency is directly correlated to the strain imposed by the coarsening process, which is not evident when considering the time and space averaged signals within the frame of previous models, where the existence of an additional dynamic process was not considered. Moreover, we find that though the occurrence of events is random in time it is not in space. Indeed, our results suggest that successive events preferentially occur at the same location.

2 Experimental

Our foam is a commercial Gillette shaving foam that consists of polydisperse bubbles tightly packed in an aqueous solution of stearic acid and triethanolamine. As demonstrated in a number of investigations,[2,7–10,12,15,19–22] this type of foam exhibits dynamical and rheological properties that are remarkably insensitive to variations in the detailed composition, which inevitably will vary as a function of the market evolution. This insensitivity denotes Gillette shaving foams as an ideal benchmark system to study different features of foam dynamics, yielding results that can be compared to the large number of prior investigations.

To characterize the coarsening process of our system, we perform both optical microscopy and diffuse light transmittance experiments.[13] Immediately after production, the foam is injected into a rectangular cell of thickness $L = 2$ mm or 5 mm and kept at a stable ambient temperature of $T = 21\,^{\circ}\mathrm{C}$. The age of the sample t_w is defined as the time elapsed since sample production. We record the evolution of the bubble size by imaging the foam surface, where we determine the mean bubble radius $\langle a_{t_w} \rangle$ based on the number of bubbles detected within the area defined by our field of view. As previously shown, $\langle a_{t_w} \rangle$ is directly proportional to the transport mean free path l^* that we measure in diffuse transmittance experiments.[2,19] To perform these experiments, we illuminate our sample with a collimated laser beam with a wavelength of 532 nm *in vacuo* and a diameter of 9 mm. A schematic layout of our experimental set-up is shown in Fig. 1. We detect the mean intensity of the transmitted light as a function of t_w using a photomultiplier and determine the age dependent transport mean free path of our sample using the transmitted intensity of a reference of known l^* to calibrate our experiment. These experiments are performed simultaneously to the diffusing wave spectroscopy experiments outlined below, which enables us to determine slight variations in the coarsening process in different runs of the experiment. By mapping the evolution of l^* to the evolution of $\langle a_{t_w} \rangle$, we find that for our foam $l^*/\langle 2 \cdot a_{t_w} \rangle = 4.6 \pm 0.3$, which is somewhat larger than the typical values found in previous experiments probing the optical properties of Gillette foams.[2,19] In agreement with previous results, we find that the bubble size evolution is well described by $\langle a_{t_w} \rangle^2 - \langle a_0 \rangle^2 \propto l^{*2}_{t_w} - l^{*2}_0 \propto t_w$, with $\langle a_0 \rangle$ and l^*_0 respectively the bubble radius and the transport mean free path at $t_w = 0$.[12,19] Our main experiments are performed at two different ages, $\bar{t_w} \cong 272$ min (age 1) and $\bar{t_w} \cong 663$ min (age 2), where $\bar{t_w}$ denotes the age of the sample at the middle of the experiment. The bubble radii are respectively $\sim$50 μm and $\sim$76 μm at age 1 and age 2. The duration of our experiments is 800 s at age 1 and 1200 s at age 2, which ensures that the bubble size does not change by more than 2% in the course of our experiments.

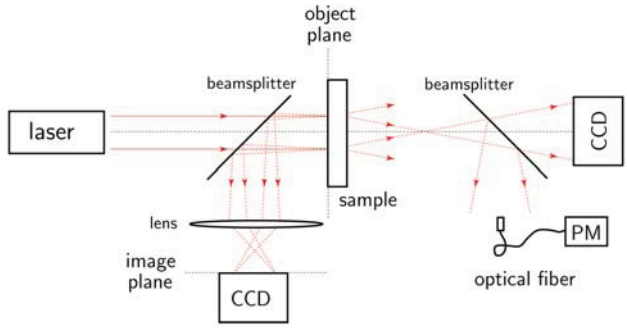

Fig. 1 Schematic of light scattering set-up used to record simultaneously the speckle pattern formed in the far-field transmission geometry and in the backscattering plane of the sample using CCD-cameras. To assess the evolution of the bubble size at each run the transmitted light intensity is measured continuously using a photo-multiplier (PM) detection scheme.

To characterize the dynamics of our foam at age 1 and age 2, we take advantage of the concepts of diffusing wave spectroscopy. Of particular relevance is the model that has been developed to describe a gradual reconfiguration of a foam by intermittent rearrangements of the local bubble configuration.[2,19] In this model, the rearrangements are presumed to occur randomly in space and time, to be instantaneous and to affect a well defined localized region of radius ξ. Assuming that all scattered light passing a rearranged region is completely dephased, while photon paths not passing through a rearranged region remain unchanged, the field autocorrelation $g_1(\tau)$ can be regarded as a direct measure of the fraction of paths not rearranged during the lag time τ; for transmission experiments $g_1(\tau)$ is then well approximated by

$$g_1(\tau) \cong \exp\{-R \cdot \tfrac{4}{3}\,\pi\,\xi^3 \cdot (L/l^*)^2 \cdot \tau\} \qquad (1)$$

with R the rate of intermittent rearrangements per unit volume. The characteristic decay time of the field correlation function $(R \cdot \tfrac{4}{3}\,\pi\,\xi^3)^{-1}$ thus denotes the mean time between events at a given location. To gain a physical intuition about the impact of a single event on $g_1(\tau)$ for a given transmission experiment, we can rewrite eqn (1) with respect to the actual volume element observed, the scattering volume V_{sc}.

$$g_1(\tau) \cong \exp\left\{-\Gamma_{V_{sc}} \cdot \frac{\frac{4}{3}\pi\,\xi^3}{V_{sc}} \cdot (L/l^*)^2 \cdot \tau\right\} \qquad (2)$$

Here, $\Gamma_{V_{sc}}$ is the rate of events occurring within the scattering volume, such that $\Gamma_{V_{sc}} \cdot \tau$ corresponds to the number of events occurring within V_{sc} during τ. The fraction of the paths randomized per event is $(\tfrac{4}{3}\,\pi\,\xi^3/V_{sc}) \cdot (L/l^*)^2$; it depends on the fraction of the scattering volume rearranged per event, $(\tfrac{4}{3}\,\pi\,\xi^3/V_{sc})$, and, due to the effective diffusion of the light through the sample, on $(L/l^*)^2$.

Our experiments are based on the classical schemes of dynamic light scattering and on the use of charge coupled device (CCD)

cameras to capture the intensity fluctuations of a large number of independent speckles simultaneously. We record the evolution of the speckle pattern in time using two different schemes.

Placing a CCD-detector far from the light-exit-plane of our sample, as shown in Fig. 1, we record the speckle pattern in the far-field transmission geometry and process the images using the time resolved correlation (TRC) scheme.[17,18] Here, we calculate a time resolved degree of correlation between two speckle patterns recorded at time t_w and $t_w + \tau$, according to

$$c_I(t_w,\tau) = \frac{1}{\beta}\left(\frac{\langle I_p(t_w)\ I_p(t_w+\tau)\rangle_p}{\langle I_p(t_w)\rangle_p \langle I_p(t_w+\tau)\rangle_p} - 1\right) \quad (3)$$

where I_p is the intensity recorded at the p-th pixel of the CCD array and $\langle\ldots\rangle_p$ denotes an average over all pixels of the speckle image; β is a prefactor that depends on the speckle-to-pixel size ratio, chosen so that $\overline{c_I(t_w,\tau)} = 1$ for $\tau \to 0$, where $\overline{\cdots}$ denotes a time average over the duration of the experiments. Note that the time averaged signal corresponds to the usual intensity correlation function $g_2(\tau) - 1 = \overline{c_I(t_w,\tau)}$, which relates to the field correlation function *via* the Siegert relation, $g_2(\tau) - 1 = g_1(\tau)^2$. The TRC-method enables us to access the temporal fluctuations in the dynamics of our samples with a spatial average taken over the entire scattering volume. The magnitude of the fluctuations due to the occurrence of local rearrangement events will here depend on the effectiveness of a single event to contribute to a decrease in $c_I(t_w,\tau)$, which we expect to depend on the fraction of the paths dephased per event; based on the model discussed above this corresponds to $(\frac{4}{3}\,\pi\,\xi^3/V_{sc})\cdot(L/l^*)^2$.

The second method used is the recently introduced photon correlation imaging technique,[16] which is closely related to other speckle imaging and near field scattering techniques.[23–26] It enables us to resolve dynamics with both temporal and spatial resolution. Instead of recording the speckle pattern in the far field, where each speckle contains phase contributions of all scatterers within the sample, we image the scattered intensity pattern at the entrance plane of the sample onto the camera, as shown in Fig. 1, and calculate the instantaneous degree of correlation with spatial resolution

$$c_I^{(s)}(t_w,\tau) = \frac{1}{\beta}\left(\frac{\langle I_p(t_w)\ I_p(t_w+\tau)\rangle_{pROI}}{\langle I_p(t_w)\rangle_p \langle I_p(t_w+\tau)\rangle_p} - 1\right) \quad (4)$$

where $\langle\ldots\rangle_{p\ ROI}$ denotes an average over pixels belonging to a region of interest (ROI) centred around the position s. The spatially resolved dynamics of the foam at a moment defined by t_w and $t_w + \tau$ can then be presented graphically by constructing dynamical activity maps, where each pixel of the map is colour coded to represent the local degree of correlation $c_I^{(s)}(t_w,\tau)$ characterizing the fluctuations of diffuse light emanating from a specific area of the sample. Examples of such dynamical activity maps are shown in Fig. 2. The occurrence of events is clearly depicted as a bright patch corresponding to a low $c_I^{(s)}(t_w,\tau)$ in the dynamical activity map, as shown for age 1 and age 2 in Fig. 2(a) and (c), respectively. As our samples are turbid, the appearance of a spatially resolved event will be limited to some critical depth within the sample, since the backscattered light is effectively diffusing on its way back to the entrance plane of the cell. To address this issue, we conduct combined backscattering and transmission experiments where we image respectively the scattered intensity pattern at the entrance and exit plane of the cell onto two identical cameras, aligning the optics so that the observation windows are the same in both geometries. We presume that spatial resolution of an event in transmission can only be obtained when the event occurs near the exit plane of the cell. Thus, if for a given cell thickness, a spatially distinct event in transmission can also be resolved in backscattering, we assess that the critical depth for the visibility of spatially resolved events is beyond the thickness L. Conducting different experiments varying L, we assess that the critical depth corresponds to $L/l^* \cong 7.5$, which is broadly consistent with estimations probing the resolution depth in speckle imaging techniques.[27]

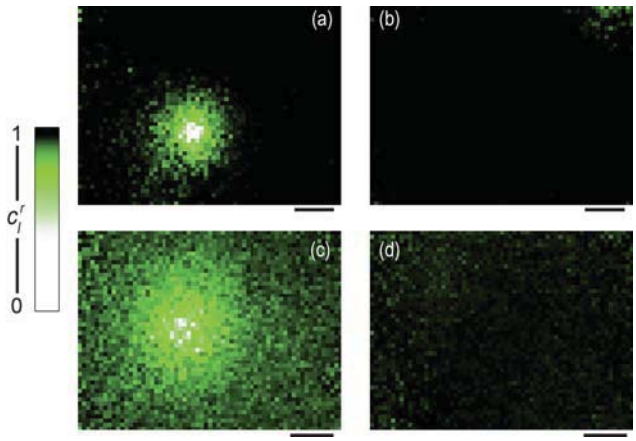

Fig. 2 Representative dynamic activity maps depicting respectively a moment at which an event occurs [(a) age 1 and (c) age 2] and a moment during the periods between events [(b) age 1 and (d) age 2]. The scale bar corresponds to 1 mm. Note that the spatial extent of the rearrangement typically scales with the bubble size.

Clearly, in both our experiments, the transmission far field and the backscattering photon correlation imaging experiment, the visibility of events depends on the thickness of the cell. To obtain the maximal visibility of the events, while still maintaining L/l^* large enough to be within the limit of the multiple scattering approximations,[28] we perform our experiments at age 1 in a cell with $L = 2$ mm and at age 2 in a cell with $L = 5$ mm. With $l^* = 0.44$ mm for age 1 and $l^* = 0.73$ mm for age 2 this corresponds to $L/l^* = 4.5$ (age 1) and $L/l^* = 6.8$ (age 2). With these L/l^* values we ensure that all events occurring throughout the depth of the sample are detected in our backscattering photon correlation imaging experiments and that the effect of a single event on $c_I(t_w,\tau)$ measured in our far field transmission TRC-experiments is maintained within the same range at both ages; here we recall that the effect of a single event on $c_I(t_w,\tau)$ scales with $(\xi^3/V_{sc})\cdot(L/l^*)^2$, where V_{sc} can be modelled by a truncated cone[13] and ξ scales with the bubble size. To be able to directly compare the temporal evolution of our signals, we perform both experiments simultaneously; in addition, the diffuse transmittance is measured continuously from $t_w \sim 0$ s to $t_w \sim 40\,000$ s, which enables us to assess the coarsening process for each run. Our CCD detectors comprise 633×483 pixels and our linear speckle size is 3 pixels in the transmission and 1 pixel in the backscattering experiments. Before each experiment we determine the exact magnification M of the image taken in the backscattering experiment by imaging

a finely marked grid that is placed at the entrance plane of our cell. Our imaging lens is placed so that $M \cong 1$, such that the observation area of our experiment is approximately 6.3×4.8 mm^2. Linear polarizers are placed in front of both cameras so that only light with a polarization perpendicular to that of the incident beam is detected; this is of particular importance in backscattering, where we thereby eliminate the shortest scattered paths and favour the detection of long, deeply probing paths. The temporal evolutions of the speckle pattern are recorded at a frequency of 50 frames/s and 25 frames/s in transmission and backscattering, respectively, where we adjust the camera exposure time between 0.1–0.3 ms depending on the average intensity level. The speckle patterns are subsequently processed to obtain the temporal evolution of both the spatially averaged signal $c_I(t_w,\tau)$ from the transmission experiments and the spatially resolved signals $c_I^{(s)}(t_w,\tau)$ that we present in dynamical activity maps. While $c_I(t_w,\tau)$ is processed at different lag-times, we analyze $c_I^{(s)}(t_w,\tau)$ for the shortest accessible experimental lag-time, $\tau = 0.04$ s, where we use the correction scheme outlined in section IV C of ref. 18 to correct for the measurement noise. The size of the region of interest over which we take the pixel average is chosen to be 0.1×0.1 mm^2, which corresponds approximately to a bubble diameter at both ages.

3 Results and discussion

Typical examples of the temporal evolution of the instantaneous degree of correlation obtained in our transmission far field experiments are shown for age 1 in Fig. 3(a) and for age 2 in Fig. 3(b). The instantaneous degree of correlation systematically decreases with increasing lag-time, indicating that at any moment in time the system exhibits dynamical activity. Indeed, the 'instantaneous' two-time correlation function can be read as a vertical cut through the data shown in Fig. 3(a) and (b); the sporadic decreases in $c_I(t_w,\tau)$ observed at both ages thus effectively indicate that the dynamical activity of our foams intermittently increases. Despite this variation, the overall time averaged correlation function $\overline{c_I(t_w,\tau)}$ exhibits a simple exponential decay, as shown in Fig. 3(c) and 3(d) for age 1 and age 2, respectively. Such exponential decay is consistent with previous experiments[2,8,19] and in principle would be consistent with the model described above, where the random intermittent restructuring of volume elements causes a decay of the correlation function that is indistinguishable to the one of continuously diffusing particles. However, as we will show, the decay of the mean correlation function is determined by at least two dynamical processes, such that this model does not fully apply for the description of the time averaged correlation function. Indeed, the inspection of the temporal evolution in the dynamical activity maps, shown as movie 1 (age 1) and movie 2 (age 2) in the ESI,† reveals that the events mostly occur one at a time in the observational volume of our experiment. Moreover, the movies clearly reveal that the local restructuring of a volume element is a rather slow process. Indeed, a characterization of the event duration by calculating the temporal correlation of the dynamical activity at a given location reveals that the events typically lasts $\tau_d = 1$ s at age 1 and $\tau_d = 1.8$ s at age 2.

Between events, the dynamical activity maps reveal that $c_I^{(s)}(t_w,\tau)$ is relatively homogeneous in space, as shown for both

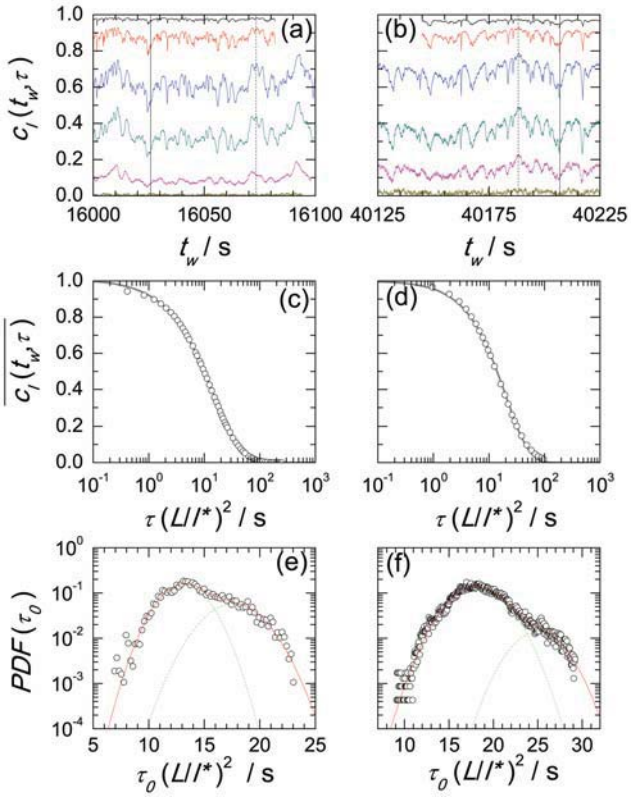

Fig. 3 Panel displaying dynamical characteristics obtained from the far field transmission experiments at age 1 (left) and age 2 (right). (a) and (b): time resolved degree of correlation as a function of t_w calculated for different lag times (a) from top to bottom: $\tau = 0.04$, 0.2, 0.68, 1.6, 4, 12 s and (b) from top to bottom: $\tau = 0.04$, 0.12, 0.32, 0.8, 1.6, 4 s. The solid and dotted vertical lines denote the moments at which the dynamical activity maps shown in Fig. 2 were acquired; the solid lines correspond to Fig. 1(a) and (c), respectively and the dotted line to Fig. 2(b) and (d). (c) and (d): time averaged correlation function as a function of lag time; to account for changes in the experimental geometry τ is normalised by $(L/l^*)^2$. The continuous lines present the results of exponential fits to the data. (e) and (f): probability density function of the 'instantaneous' decay time $\tau_0(t_w)$ obtained by fitting the age dependent two-time correlation function to eqn (5). The continuous red lines present the sum of two Gaussian distributions (green dashed line) that are used to fit the data.

ages in Fig. 2(b) and Fig. 2(d). The direct comparison of the results obtained in our photon correlation imaging experiment to those obtained in the simultaneously performed TRC-experiments shows that the fluctuations in the TRC-traces are effectively caused by single events of finite duration. However, during the event-free periods the spatially averaged dynamics probed in our transmission experiments is not suppressed. This can be seen for instance at the moments that are marked by a dotted line in Fig. 3(a) and Fig. 3(b), which are the moments at which the dynamical activity maps shown in Fig. 2(a) and (c) were acquired. Clearly, $c_I(t_w,\tau)$ still fully decays during these event-free periods, which indicates that another dynamical process contributes to the dephasing of the scattered light. As this process does not lead to significant fluctuations in the degree of correlation, neither in space nor in time, we assume that this dynamics is quasi-continuous and occurs everywhere within the

sample. Our findings are consistent with the findings obtained in recent speckle visibility experiments, where both the finite duration of the event and the existence of an addition dynamical process were detected as well.[15] However, in contrast to the speckle visibility technique, the TRC-technique allows us to assess the full lag-time dependence of the different dynamical processes contributing to the dephasing of the scattered light. As both the duration of the events and the event-free periods between events are rather long compared to the experimental decay time of the time-averaged intensity correlation function, we can attempt to isolate the contribution of the quasi-continuous process by fitting the two-time correlation function with

$$c_I(t_w,\tau) = \frac{1}{\beta(t_w)}\exp\left\{-\left(\tau/\tau_0(t_w)\right)^{p(t_w)}\right\} \quad (5)$$

where we allow the intercept $1/\beta(t_w)$, the decay time $\tau_0(t_w)$ and the stretching exponent $p(t_w)$ to vary with t_w. At both ages we find that the probability density functions (PDF) of the instantaneous decay times $\tau_0(t_w)$ exhibit the same basic features: at shorter decay times the $PDF(\tau_0)$ exhibits a reasonably well-defined maximum, at larger decay times the $PDF(\tau_0)$ is characterized by a shoulder, as shown for age 1 in Fig. 3(e) and for age 2 in Fig. 3(f), where we normalize the decay times with $(L/l^*)^2$ to account for the varying experimental conditions. Our results clearly show that the decay of the mean-correlation function is the result of two processes with different characteristic times. Indeed, we can attribute the time scale of the second maximum to the one characterizing the quasi-continuous process, while the time scale of the first maximum still constitutes a convolution of both the restructuring events and the quasi-continuous process. In order to determine the characteristic time describing the quasi-continuous process τ_c, we fit the PDFs to a pair of Gaussian distributions that we find to describe the data reasonably well, as shown by the red continuous line in Fig. 3(e) and (f). From the resulting fit parameter $\tau_{0,max2}\cdot(L/l^*)^2$, we determine $\tau_c = 2\cdot\tau_{0,max2}\cdot(L/l^*)^2$ and report the results in Table 1; for better comparison to the original model outlined above (see eqn (1) and 2) we choose to consistently state decay times that apply to the decay of the field correlation function rather than the intensity correlation, which just entails to apply a factor of two to the decay time of the intensity correlation function. As compared to the mean decay-time $\tau_m = 2\cdot\tau_0\cdot(L/l^*)^2$ determined from the exponential fit to the data shown in Fig. 3(c) and (d), τ_c is larger by a factor of ~1.2 and ~1.5 for age 1 and age 2 respectively. Interestingly, such moderate change in the decay time of the correlation function was also reported for experiments probing the foam dynamics before and after a large oscillatory shear strain was applied.[8] Presuming that a large oscillatory shear strain erases internal stress imbalances, such that the rearrangement events are temporally suppressed, it is likely that the residual dynamics observed after the application of shear corresponds to the quasi-continuous dynamics observed here between events. This would suggest that the quasi-continuous process is not directly linked to the release of imbalanced stresses.

Finally, we note that the age dependence of the quasi-continuous process does not correspond to the one of the mean dynamics, as denoted by comparing the ratios τ_m(age 2)/τ_m(age 1) and τ_c(age 2)/τ_c(age 1) listed in Table 1. This indicates that the event dynamics contributes to the mean dynamics so that the age-dependence is altered. Moreover, an inspection of the correlation between $\tau_0(t_w)$ and $p(t_w)$ reveals that the quasi-continuous process is best described by a slightly compressed exponential, while during the occurrence of events the decay of the two time correlation function is described by a slightly stretched exponential. It is indeed remarkable that this combination between fast and stretched decays and slow and compressed decays leads to a simple exponential decay in the mean correlation function. However, this high degree of convolution of event dynamics and quasi-continuous dynamics determining the mean dynamics significantly hinders the characterization of the rate of topological rearrangements and consequently their dependence on the coarsening process.

By contrast, the characterization of the event dynamics is rather straightforward using the results of our photon correlation imaging experiments. Indeed, the temporal evolution of the events can simply be followed in movies like the one shown in the ESI.† Just counting the events allows us to determine the event rate per unit volume R reported in Table 1, where we estimate the size of our observational volume as the product of the size of the field of view of our camera and the thickness of the cell. Clearly, the event rate within a given volume is significantly larger at age 1 than at age 2. However, to evaluate Γ_r the rate at which a volume element is effectively restructured, we need to account for the number of possible rearrangement zones within our observation volume, which scales with the age-dependent size of the rearranged zone ξ. An analysis of the event size, by calculating the spatial correlation of $c_I^{(s)}(t_w,\tau)$ introduced as $\tilde{G}_4(\Delta s,\tau)$ in ref. 16, reveals that ξ scales with the bubble size and extends over ~10 bubble diameters, in agreement with previous assessments.[2,15,19] The large spatial extent and long durations of the events observed in our experiments are consistent with the events probed at the foam surface, where we observe that a series of neighbour-switching events, T1-events,[1] rearranges a zone extending over ~ 4 bubble diameters. The even larger size of the

Table 1 Comparison of coarsening and dynamical characteristics of Gillette foam at two different ages. $\overline{t_w}$ age of the sample at the middle of the experiment; $\langle a_{t_w}\rangle$ mean bubble radius; $d\langle a_{t_w}\rangle/dt$ rate of bubble growth; $d\gamma/dt$ strain rate set by the coarsening process; τ_m characteristic decay time of the time and spatially averaged field auto-correlation function; τ_c decay time characterizing the quasi-continuous process; R rate of events per unit volume obtained from counting procedure; Γ_r restructuring rate obtained from counting procedure; τ_d duration of intermittent events.

		Age 1	Age 2	Age 1/Age 2
$\overline{t_w}$	[min]	272	663	
$\langle a_{t_w}\rangle$	[μm]	50	76	
$d\langle a_{t_w}\rangle/dt$	[μm s^{-1}]	1.05×10^{-3}	0.88×10^{-3}	1.19
$d\gamma/dt$	[s^{-1}]	6.87×10^{-5}	3.40×10^{-5}	2.02
τ_m	[s]	29.9	35.0	
τ_m	[s^{-1}]	33.4×10^{-3}	28.6×10^{-3}	1.17
τ_c	[s]	35.2	51.8	
τ_c	[s^{-1}]	28.4×10^{-3}	19.3×10^{-3}	1.47
R	[s^{-1} mm^{-3}]	13.5×10^{-3}	1.80×10^{-3}	
Γ_r	[s^{-1}]	4.52×10^{-4}	2.12×10^{-4}	2.13
τ_d	[s]	1.0	1.8	

event observed in diffusing wave spectroscopy can be understood as that the event typically contains both a central volume element, in which the bubbles topologically reconfigure, and a halo of bubbles that respond elastically without rearranging, such that the zone that effectively contributes to the dephasing of light extends over ~10 bubble diameters.[2,8,15]

To evaluate the restructuring rate, we thus assume that the size of the effectively topological rearranged zone is $\xi = 4 <a_t>$. As shown in Table 1, $\Gamma_r = R \cdot {}^4\!/_3\ \pi\ (4 < a_{tw} >)^3$ decreases by approximately a factor of 2.1 from age 1 to age 2. To assess the relation between the topological rearrangements and the coarsening process, we evaluate the strain rate set by the coarsening process as $d\gamma/dt \approx (\Delta V/V)/\Delta t$, with V and $\Delta V/\Delta t$ respectively the bubble volume and the change of the bubble volume per unit time at a given foam age. As shown in Table 1, we find that the ratio of the age dependent strain rates $[(d\gamma/dt(\text{age 1}))/(d\gamma/dt(\text{age 2})) = 2.02]$ correspond, within the experimental error, to the ratio of the restructuring rates $[\Gamma_r(\text{age 1})/\Gamma_r(\text{age 2}) = 2.1]$. This strongly suggests that the events are a direct result of the coarsening induced strain between events. Estimating this critical strain as $\gamma_y = (d\gamma/dt)/\Gamma_r$, we find that $\gamma_y \sim 0.16 \pm 0.01$ in reasonable agreement with the critical strain measured for our foams in experiments probing the macroscopic mechanical properties. This correlation between strain rate and event rate is not evident when considering the decay rates of the mean correlation function τ_m^{-1}, which, following eqn (1) $[\tau_m^{-1} = R \cdot ({}^4\!/_3\ \pi\ r^3)]$, should effectively correspond to the restructuring rates if the dynamic light scattering signal would be determined by the random restructuring of volume elements only. Here the ratio $\tau_m^{-1}(\text{age 1})/\tau_m^{-1}(\text{age 2})$ would appear to correlate to the ratio of the bubble growth rather than to that of the strain rates, as shown in Table 1. Indeed, the convolution of event-frequency, event duration and quasi-continuous dynamics that all exhibit a different age-dependence leads to an age-dependence in the mean-dynamics that is unsuitable for establishing relations between the coarsening process and topological rearrangements.

To address the question whether not the disappearance of bubbles, T2-events,[1] rather than the mean strain set by the coarsening process is at the origin of the mechanical instabilities that lead to the intermittent rearrangements observed, we estimate the number of bubbles disappearing within a time interval Δt as

$$N_b(t_w) - N_b(t_w + \Delta t) = \frac{3}{4\pi}\left(\frac{1}{<a(t_w)>^3} - \frac{1}{<a(t_w + \Delta t)>^3}\right) \quad (6)$$

where $N_b(t_w)$ and $N_b(t_w + \Delta t)$ are respectively the number of bubbles per unit volume at an age of t_w and $t_w + \Delta t$. This estimate yields a rate for T2-events per unit volume that exceeds the rate of events per unit volume R by a factor of ~10, such that it appears unlikely that T2-events are at the actual origin of the events observed. Finally, we note that single T2-events are small and involve the motion of only a few plateau-borders, which have been previously identified to be the principal scattering sites in dry foams.[29] T2-events are thus unlikely to be resolved in our experiments, as the resolution is limited by the number of paths rearranged by an event divided by the total number of paths contributing to $c_I^{(s)}(t_w,\tau)$ of a given ROI.

To further progress in our understanding of the topological rearrangements, we characterize the temporal and spatial distribution of the events exploiting the temporally resolved dynamical activity maps. We assess the time at which an event occurs as the moment where the dynamical activity is maximal during an event. At this moment, the location of the event is determined as the centre of the high dynamical activity zones, as those shown in Fig. 2(a) and (c). The results obtained from our analysis of the experiment at age 1 are shown in Fig. 4; qualitatively similar results are obtained for the experiment at age 2, but the quality of the data is somewhat lower as the number of events probed over the duration of our experiment is here lower than at age 1. In agreement with previous results,[15] we find that the time delay between successive events Δt_e follows an exponential distribution, as shown in Fig. 4(a). This is consistent with the Poissonian statistics expected for the random occurrence of independent events. To characterize the distribution of the events in space we determine the distance, r, between the i^{th} and $(i + n)^{th}$ event and calculate the probability density function of r, $PDF(r)_{experiment}$, for a given n. To account for the limited geometry of our experiment we determine the PDF expected for a random distribution of events in space $PDF(r)_{random}$ using simulations, where we implement the experimental boundary conditions. By normalising $PDF(r)_{experiment}$ with $PDF(r)_{random}$, we obtain the radial distribution function $g(r) = PDF(r)_{experiment}/PDF(r)_{random}$, where we expect $g(r) = 1$ at all r for a random distribution events in space. Instead, we find that $g(r) > 1$ for small r and $n < 30$, as shown in Fig. 4(b); as the decay of $g(r)$ varies only slowly with increasing n we have here averaged each $g(r)$ over a few values of n to reduce the statistical fluctuations. The increased probability at small r indicates that the foam maintains a spatial "memory" of its dynamics; the occurrence of an event at a given location is thus correlated to previous rearrangements although no temporal correlation is observed. The intercept of $g(r)$ decreases with increasing n, indicating that the structural memory effect weakens with time. Moreover, we note that $g(r)$ decreases to the background level at r corresponding to

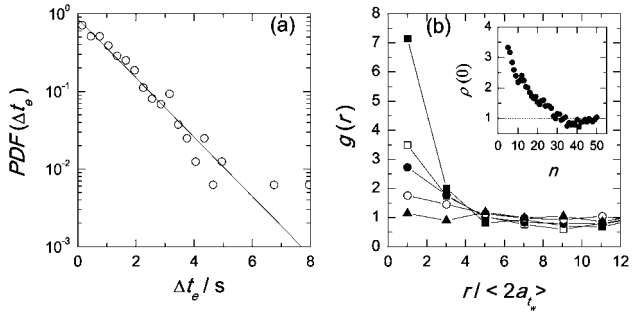

Fig. 4 (a) Probability density function of time delay between successive events. The solid line denotes the exponential behaviour expected for the random occurrence of independent events. (b) Experimentally determined probability to find the $(i + n)^{th}$ event observed within our experimental volume at a distance r from the i^{th} event normalized by the probability expected for randomly distributed events, $g(r) = PDF(r)_{experiment}/PDF(r)_{random}$. As $g(r)$ varies smoothly with increasing n, $g(r)$ obtained for n = 1–5 (filled squares), n = 6–10 (open squares), n = 11–15 (filled circles), n = 16–20 (open circles), and n = 36–40 (triangles) are averaged to reduce the statistical fluctuations. Inset: Probability that the $(i + n)^{th}$ event observed within our observational volume is located within the topologically rearranged zone of the i^{th} event divided by the expectation value for randomly distributed events.

4–5 bubble diameters; this indicates that the actual centre of an event is likely to be located within the topologically rearranged zone of a previous event. To quantify the time over which events are more likely to occur within such zone, we integrate $g(r)$ for r up to 4 bubble diameters. The integrated value, $\rho(0)$, compares the experimentally found event probability within an already rearranged zone of size $r = 4$ bubble diameters to that of randomly distributed events. It decreases slowly with n, reaching unity at $n \cong 30$, as shown in the inset of Fig. 4(b), where we have used a five-point moving average to smooth the data. Corresponding to $n \cong 30$, the spatial memory time of an event would thus extend up to $\sim$30 s; using this time to evaluate the mean strain set by the coarsening process we find a strain that is 2 orders of magnitudes lower than γ_y.

These findings suggest that a fragile bubble configuration is likely to still be fragile after reconfiguration. Indeed, if we consider that the coarsening process leads to imbalances in the stress-configuration, an event will be set off where the excess stress exceeds the local yield stress. The reconfiguration process will proceed until the excess stress is again below the yield stress; this, however, implies that the excess stress of the recently rearranged zone is just below the yield stress. As the coarsening process continuously perturbs the stress configurations throughout the system, the likelihood that the yield stress within this zone is soon going to be exceeded again is then high, consistent with the observed behaviour. An increased probability to find an event within the already rearranged zone is also enclosed in the fact that the topological rearrangement leads to an elastic deformation of the surroundings. Indeed, this elastic response is likely to further contribute to the unfavourable stress balance within the just rearranged zone. These conditions denote that coarsening induced rearrangements are fairly inefficient in relaxing unbalanced stress configurations and thus suppressing rearrangements. This contrasts with the effect of imposing large macroscopic oscillatory strains, which has been shown to efficiently suppress the occurrence of rearrangement events.[8,12] Indeed, imposing a strain that significantly exceeds the yield strain leads to a reconfiguration of the ensemble of the bubbles; both the initiation and cessation of bubble rearrangements are here not governed by threshold configurations; moreover, the topological reconfiguration of the ensemble eliminates the effect of the elastic deformation, such that fragility is not preserved.

Finally, we note that a persistence of stress-imbalances within a given region has been recently inferred from experiments probing the spatial heterogeneities in the dynamics of compressed microgel systems.[5] There it was observed that well-localized zones of high dynamical activity coexisted with zones of low dynamical activity and that the high dynamical activity within a zone persisted in time, which indicates that rearrangements not necessarily lead to a balanced stress configuration.

To some extent this behaviour is reminiscent of dynamical facilitation in glasses, where an immobile zone can only become mobile when the neighbouring zone is already mobile.[30] As a direct consequence of the highly cooperative nature in the dynamics of glassy systems the onset of mobility in a given zone correlates here to the mobility of the neighbouring zone. In foams, the onset of mobility in a given zone correlates to previous mobility within the same zone. One may speculate that both correlations are related to the actual origin of the dynamics in glasses and deeply jammed systems. While the thermally-driven dynamics in glasses imposes cooperativity, *i.e.* fluidization of a neighbouring region, rearrangements driven by unbalanced stresses in deeply jammed systems increase the 'degree of jamming' in the surroundings, thereby inducing an imbalance of internal stresses at the location that has just been rearranged.

4 Conclusions

In conclusion, we have investigated spatial and temporal heterogeneities in the dynamics of a coarsening foam at two different ages, conducting simultaneously experiments in the transmission and backscattering geometry of diffusing wave spectroscopy. In transmission, we performed the experiments in the traditional far field limit, while we used the photon correlation imaging configuration[16] in the backscattering experiments. The combination of these experiments allows us to critically address different contributions to the dynamic light scattering signal. In agreement with previous experiments,[15] we find that the foam dynamics is determined by two processes: intermittent bubble rearrangements of finite duration and a quasi-continuous process that is spatially homogeneous. Both processes contribute to the dynamic light scattering signal, which significantly complicates the interpretation of the mean signal. For the characterization of the event dynamics, it becomes evident that the photon correlation imaging technique is a particularly useful tool, as it provides the means to assess both the frequency and the position of the events without the need of modelling the actual magnitude of the dynamic light scattering signal. These experiments reveal that the event frequency is directly correlated to the strain-rate imposed by the coarsening process, which indicates that the events are triggered by a well defined strain. Our analysis of the spatial correlation between successive events uncovers that the events are not randomly distributed in space. Indeed, we find that the probability to find an event at a location that has been previously rearranged is significantly higher than expected for a random spatial distribution of events. This unexpected behaviour indicates that a locally unstable zone rearranges to a state that is just below the yield stress, such that the likelihood that this zone is soon going to be again rearranged is high. Such persistence might be a general characteristic of stress-driven dynamics that could be observed in other jammed systems where the direct contact between the constituents may result in an unbalanced stress-configuration.

Our findings evoke several interesting questions that could be addressed in future experiments. In particular, the experiments probing the effect of a macroscopic applied strain could be used to explore the fragility of a rearranged zone. One could envision that a small oscillatory strain would facilitate the secondary events, such that the events would merge within the typical duration of a single event; in such a case it is likely that the spatial distribution of events would appear to be random. Moreover, it would be interesting to investigate the evolution of the spatial heterogeneities in the dynamics of a foam that has been subjected a large external shear, as this has been done for the mean dynamics in ref. 8,12. Such investigations should help to assess the efficiency of restructuring events in equilibrating stress

imbalances and could lead to a better understanding of the quasi-continuous process whose origin remains unclear.

5 Acknowledgements

This work has been supported by the Swiss National Science Foundation, the CNES (ACI No. JC2076) and CNRS (PICS No. 2410). L. C. acknowledges support from the Institut Universitaire de France. We thank Douglas J. Durian, Reinhard Höhler and David A. Weitz for fruitful discussions.

6 References

1 D. Weaire and S. Hutzler, '*The Physics of Foams*', Clarendon Press, 1999.
2 D. J. Durian, D. A. Weitz and D. J. Pine, *Science*, 1991, **252**, 686.
3 P. Sollich, F. Lequeux, P. Hebraud and M. E. Cates, *Phys. Rev. Lett.*, 1997, **78**, 2020.
4 L. Cipelletti, S. Manley, R. C. Ball and D. A. Weitz, *Phys. Rev. Lett.*, 2000, **84**, 2275.
5 D. A. Sessoms, I. Bischofberger, L. Cipelletti and V. Trappe, *Philos. Trans. R. Soc. London, Ser. A*, 2009, **367**, 5013.
6 L. Ramos and L. Cipelletti, *Phys. Rev. Lett.*, 2005, **94**, 158301.
7 J. C. Earnshaw and A. H. Jaafar, *Phys. Rev. E: Stat. Phys., Plasmas, Fluids, Relat. Interdiscip. Top.*, 1994, **49**, 5408.
8 A. D. Gopal and D. J. Durian, *Phys. Rev. Lett.*, 1995, **75**, 2610.
9 A. D. Gopal and D. J. Durian, *J. Opt. Soc. Am. A*, 1997, **14**, 150.
10 R. Höhler, S. Cohen-Addad and H. Hoballah, *Phys. Rev. Lett.*, 1997, **79**, 1154.
11 A. D. Gopal and D. J. Durian, *J. Colloid Interface Sci.*, 1999, **213**, 169.
12 S. Cohen-Addad and R. Höhler, *Phys. Rev. Lett.*, 2001, **86**, 4700.
13 D. A. Weitz and D. J. Pine, in *Diffusing-wave spectroscopy*, ed. W. Brown, Clarendon Press, Oxford, 1993.
14 G. Maret, *Curr. Opin. Colloid Interface Sci.*, 1997, **2**, 251.
15 A. S. Gittings and D. J. Durian, *Phys. Rev. E: Stat., Nonlinear, Soft Matter Phys.*, 2008, **78**, 066313.
16 A. Duri, D. A. Sessoms, V. Trappe and L. Cipelletti, *Phys. Rev. Lett.*, 2009, **102**, 085702.
17 L. Cipelletti, H. Bissig, V. Trappe, P. Ballesta and S. Mazoyer, *J. Phys.: Condens. Matter*, 2003, **15**, S257.
18 A. Duri, H. Bissig, V. Trappe and L. Cipelletti, *Phys. Rev. E: Stat., Nonlinear, Soft Matter Phys.*, 2005, **72**, 051401.
19 D. J. Durian, D. A. Weitz and D. J. Pine, *Phys. Rev. A: At., Mol., Opt. Phys.*, 1991, **44**, R7902.
20 S. Cohen-Addad, H. Hoballah and R. Höhler, *Phys. Rev. E: Stat. Phys., Plasmas, Fluids, Relat. Interdiscip. Top.*, 1998, **57**, 6897.
21 R. Höhler, S. Cohen-Addad and A. Asnacios, *Europhys. Lett.*, 1999, **48**, 93.
22 S. Cohen-Addad, R. Höhler and Y. Khidas, *Phys. Rev. Lett.*, 2004, **93**, 028302.
23 J. D. Briers, *Opt. Appl.*, 2007, **37**, 139.
24 P. Zakharov and F. Scheffold, *Soft Mater.*, 2010 to appear.
25 M. Erpelding, A. Amon and J. Crassous, *Phys. Rev. E: Stat., Nonlinear, Soft Matter Phys.*, 2008, **78**, 046104.
26 R. Cerbino and A. Vailati, *Curr. Opin. Colloid Interface Sci.*, 2009, **14**, 416.
27 P. Zakharov, A. Völker, A. Buck, B. Weber and F. Scheffold, *Opt. Lett.*, 2006, **31**, 3465.
28 P. D. Kaplan, M. H. Kao, A. G. Yodh and D. J. Pine, *Appl. Opt.*, 1993, **32**, 3828.
29 M. U. Vera, A. Saint-Jalmes and D. J. Durian, *Appl. Opt.*, 2001, **40**, 4210.
30 J. P. Garrahan and D. Chandler, *Phys. Rev. Lett.*, 2002, **89**, 035704.